Geomechanics and Engineering, *Vol. 23, No. 3 (2020) 207-215*
DOI: https://doi.org/10.12989/gae.2020.23.3.207

Passive earth pressure for retaining structure considering unsaturation and change of effective unit weight of backfill

Li Zheng[1], Lin Li*[1], Jingpei Li[1] and De'an Sun[2]

[1]Department of Civil Engineering, Tongji University, Shanghai 200092, China
[2]Department of Civil Engineering, Shanghai University, Shanghai 200444, China

(Received May 10, 2020, Revised September 16, 2020, Accepted October 8, 2020)

Abstract. This paper presents a kinematic limit analysis for passive earth pressure of rigid retaining structures considering the unsaturation of the backfill. Particular emphasis in the current work is focused on the effects of the spatial change in the degree of saturation on the passive earth pressure under different steady-infiltration/evaporation conditions. The incorporation of change of effective unit weight with degree of saturation is the main contribution of this study. The problem is formulated based on the log-spiral failure model rather than the linear wedge failure model, in which both the spatial variations of suction and soil effective unit weight are taken into account. Parametric studies, which cover a wide range of flow conditions, soil types and properties, wall batter, back slope angle as well as the interface friction angle, are performed to investigate the effects of these factors on the passive pressure and the corresponding shape of potential failure surfaces in the backfill. The results reveal that the flow conditions have significant effects on the suction and unit weight of the clayey backfill, and hence greatly impact the passive earth pressure of retaining structures. It is expected that present study could provide an insight into evaluation of the passive earth pressure of retaining structures with unsaturated backfills.

Keywords: passive earth pressure; retaining structure; unsaturation; suction; log spiral failure model

1. Introduction

Design of retaining structures often requires calculation of the resultant force of lateral earth pressure distribution. It's commonly assumed that the backfill is dry or fully saturated in the classical earth pressure theories, such as the Rankine's theory of earth pressure and Coulomb's theory of earth pressure (Coraig 2004). These theories simplify the stress state of soil without considering the unsaturated zone above the water table. However, ignoring the unsaturated features of soil, such as the spatial changes of the suction and soil effective unit weight under different flow conditions, which potentially impacts the earth pressure, will cause an increasing risk of failure for retaining structures (e.g., Yoo and Jung 2006, Koerner and Koerner 2013, Valentine 2013, Vahedifard *et al.* 2014) and instability of the slopes (e.g., Rahardjo *et al.* 2008, Godt *et al.* 2009, Michalowski and Drescher 2009, Damiano *et al.* 2012, Gao *et al.* 2013, 2016, Keskin and Laman 2014, Yang and Xu 2017; Yamaguchi *et al.* 2018, Yang and Liu 2018).

The significant effects of unsaturation of the backfill motivate a need for developing more advanced approaches to calculate the lateral earth pressures, such as the limit equilibrium method (e.g., Vahedifard *et al.* 2015, Sahoo and Ganesh 2017, Deng and Yang 2019), limit analysis method (e.g., Soubra 2000, Lancellotta 2007, Zhao *et al.* 2009, Shwan *et al.* 2016) and the finite element method (e.g., Lim *et al.* 2015, Krabbenhoft 2017, Veiskarami *et al.* 2018, Fathipour *et al.* 2020). The limit analysis method has advantage of simplicity without loss of strict theoretical basis, but the difficulty lies in constructing possibly kinematically admissible mechanisms. With the limit analysis method, Soubra (2000) investigated the passive earth pressure problem by proposing a sequence of rigid triangles translational kinematically admissible failure mechanism in dry soils; Shwan (2016) extended the computational limit analysis method and discontinuity layout optimization (DLO) to analyze the passive earth pressure under unsaturated soils. Finite element method can incorporate the features of unsaturated soil and hence is capable of properly reflecting the critical failure mechanism without prescribing a particular failure surface in the backfill. Krabbenhoft (2017) and Veiskarami *et al.* (2018) employed upper/lower bound finite element limit analysis (FELA) to evaluate the seismic earth pressure in isotropic and anisotropic dry soils, respectively. Fathipour *et al.* (2020) further combined the FELA with the unified effective stress approach to evaluate the lateral earth pressures in unsaturated soils. However, the high requirements of expertise to perform these numerical simulations limit their wider application. In contrast, the suction-based effective stress representation (Lu and Likos 2006) makes it possible to incorporate the suction of the unsaturated backfill into the limit analysis so as to analyze the lateral earth pressure of the retaining structures. With the suction-based effective stress, Vahedifard *et al.* (2015) investigated the active earth pressures on the retaining wall under different flow conditions based on the limit analysis employing a log-spiral surface. Sahoo and Ganesh (2017)

∗Corresponding author, Ph.D.
E-mail: 1310230@tongji.edu.cn

http://www.techno-press.org/?journal=gae&subpage=7
ISSN: 2005-307X (Print), 2092-6219 (Online)

assumed a planar slip surface for analysis of active earth pressure and compared the results with Vahedifard *et al.* (2015). Deng and Yang (2019) calculated passive earth pressures for unsaturated soils based on similar approach to Sahoo and Ganesh (2017). The results of these analyses showed that the change of the suction due to infiltration/evaporation has pronounced effects on the lateral earth pressure acting on the retaining structures, especially for the clayey backfills. This sufficiently highlights the importance of considering the unsaturation of the backfill in assessing the active/passive earth pressures for retaining structures. However, the change of the unit weight of the backfill due to infiltration/evaporation, which also has pronounced effects on the active earth pressures, is not involved in their analysis. Hence, it is of great significance to develop a kinematic limit analysis method that incorporates the effects of both suction and unit weight for evaluation of the earth pressure on retaining structures.

This paper presents a kinematic limit analysis on the passive resistance of retaining structures with unsaturated backfill under different flow conditions The salient feature of present study lies in that the changes of spatial distributions of suction and soil effective unit weight due to infiltration/evaporation are properly incorporated in the present kinematic limit analysis method. Another advantage of the present kinematic limit analysis is that the log-spiral failure model, instead of the linear wedge failure model, is developed for evaluating the passive earth pressure of retaining structures. The incorporation of the effects of unite effective unit weight with degree of saturation on the passive earth pressure is the main contribution of present study. The proposed method is validated by comparing the results with the well-documented data from Deng and Yang (2019). On the basis of the present kinematic limit analysis, parametric studies are conducted to investigate the effects of the flow conditions, the soil types and properties, the wall batter, the back slope angle and the interface friction angle on the passive resistance of the retaining structures. This study would provide a theoretical base for evaluation of the passive earth pressure of retaining structures with unsaturated backfills.

2. Spatial characteristics of unsaturated soil under steady flow condition

2.1 Spatial distribution of suction

The unified effective stress for unsaturated soil proposed by Lu and Likos (2006) is employed in this study to represent the effective stress of the unsaturated backfills. The unified effective stress introduces the effective degree of saturation and the SWRC (soil-water retention curve) in the bishop's effective stress to consider the realistic suction of the unsaturated soils, which is expressed as

$$\sigma' = \sigma - u_{\mathrm{a}} - \sigma^{\mathrm{s}} \tag{1}$$

where σ' is the effective stress of soil; σ is the total stress of soil; u_{a} is the pore-air pressure; σ^{s} represents the suction of the unsaturated soil. Lu et al (2010) proposed a closed-form equation for suction stress σ^{s} as a function of

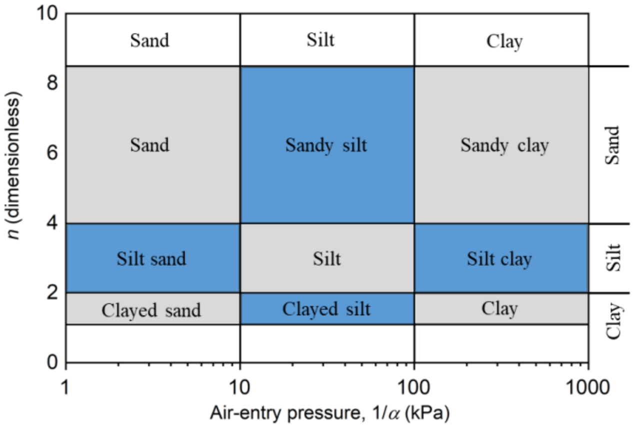

Fig. 1 Typical classification for soils with parameters α and n (Lu *et al.* 2010)

matric suction with two fitting parameters α and n defined by van Genuchten (1980) and Mualem (1976) from SWCC, which are given as follows

$$\sigma^{\mathrm{s}} = -(u_{\mathrm{a}} - u_{\mathrm{w}}) \qquad (u_{\mathrm{a}} - u_{\mathrm{w}}) \le 0 \tag{2a}$$

$$\sigma^{\mathrm{s}} = -\frac{(u_{\mathrm{a}} - u_{\mathrm{w}})}{\{1 + [\alpha(u_{\mathrm{a}} - u_{\mathrm{w}})]\ \}^{\frac{-1}{}}} \qquad (u_{\mathrm{a}} - u_{\mathrm{w}}) \ge 0 \tag{2b}$$

where α approximates the inverse of the air-entry pressure and typically varies between 0 and 0.5 kPa-1; n is related with the distribution of pore size of soil and generally lies between 1.1 and 8.5 for most soils. Fig. 1 presents the typical classification of soils with different values of α and n (Lu *et al.* 2010). The notation $u_{\mathrm{a}} - u_{\mathrm{w}}$ is matric suction, u_{a} indicates the pore-air pressure, which generally equals to the atmospheric pressure and is measured as zero (Vahedifard *et al.* 2015), u_{w} is the pore water pressure.

The magnitude of matric suction $u_{\mathrm{a}} - u_{\mathrm{w}}$ is affected by the flow conditions, such as infiltration or evaporation. Hence, the situation that the backfill behind the retaining structure under one-dimensional vertical steady flow is considered in this study. Based on Darcy's law and Gardner's (1958) model, Lu and Likos (2004) proposed an analytical solution for the matric suction under vertical steady flow as follows

$$(u_{\mathrm{a}} - u_{\mathrm{w}}) = -\frac{1}{\alpha}\mathrm{In}\left[\left(1 + \frac{q}{k_{\mathrm{s}}}\right)e^{-\alpha\gamma_{\mathrm{w}}(z+z_0)} - \frac{q}{k_{\mathrm{s}}}\right] \tag{3}$$

where q is the vertical specific discharge, of which positive value for evaporation, negative value for infiltration and zero for no-flow condition; k_{s} is the saturated hydraulic conductivity, which depends on soil type and void ratio of the soil; z_0 is the constant vertical distance from the water table to the toe elevation of the slope, this study assumes that the water table is at the elevation of the slope toe; z represents the distance from the toe elevation of slope to the calculated point of matric suction.

Substituting Eq. (3) into Eq. (2b), the equation that describes the spatial distribution of the suction in the backfill under steady flow can be obtained as

$$\sigma^s = \frac{\ln\left[\left(1+\frac{q}{k_s}\right)e^{-\alpha\gamma_w(z+z_0)} - \frac{q}{k_s}\right]}{\alpha\left(1+\left\{-\ln\left[\left(1+\frac{q}{k_s}\right)e^{-\alpha\gamma_w(z+z_0)} - \frac{q}{k_s}\right]\right\}^n\right)^{\frac{n-1}{n}}} \quad (4)$$

It can be seen from Eq. (4) that, the value of suction stress is negative under vertical steady flow condition. The steady flow condition makes it possible to develop an analytical solution of suction stress into the kinematic limit equilibrium method to evaluate the passive resistance of the retaining structures.

2.2 Spatial distribution of soil effective unit weight

The effective unit weight of unsaturated soil is also affected by the degree of saturation and vertical flows. Van Genuchten (1980) defined the effective degree of saturation S_e, which relates with matric suction $u_a - u_w$, as follows

$$S_e = \frac{S - S_r}{1 - S_r} = \frac{1}{\{1 + [\alpha(u_a - u_w)]^n\}^{\frac{n-1}{n}}} \quad (5)$$

where S indicates the pore-water degree of saturation; S_r is the residual saturation, which is explained as the water content induced by soil particle hydration. Therefore, the value of S_r is relatively small. The testing values of S_r for different types of soil along wetting path were given by Lu *et al.* (2013). In this study $S_r = 0.1$ is adopted for simplification of the analysis.

On the other hand, the effective unit weight of soil γ' can be given according to the relationship of gases, liquid, and solid phases of unsaturated soils as follows

$$\gamma' = \frac{G_s + [S_r + (1 - S_r)S_e]}{1 + e}\gamma_w \quad (6)$$

where G_s represents the specific gravity of soil. Previous studies (Prakash *et al.* 2012) showed that the value of G_s normally falls in the range of 2.6 to 2.8 for most silt and clays and this study assumes $G_s = 2.7$. e is the porosity ratio of soil and can be calculated as

$$e = \frac{G_s\gamma_w - \gamma_{sat}}{\gamma_{sat} - \gamma_w} \quad (7)$$

where γ_{sat} and γ_w are the unit weight of saturated backfill and water respectively, which are set as 20 kN/m^3 and 10 kN/m^3 in this study.

Substituting Eqs. (3), (5) and (7) into Eq. (6), the expressions for the spatial distribution of the effective unite weight of the backfill under vertical steady flow can be given as

$$\gamma' = \frac{G_s\gamma_w}{1+e} + \gamma_w\left[\frac{S_r\{1+[\alpha(u_a-u_w)]^n\}^{\frac{n-1}{n}} + (1-S_r)}{(1+e)\{1+[\alpha(u_a-u_w)]^n\}^{\frac{n-1}{n}}}\right]\frac{G_s\gamma_w - \gamma_{sat}}{\gamma_{sat} - \gamma_w} \quad (8)$$

Fig. 2 shows the spatial distributions of suction and effective unit weight of clay backfill ($n = 2, \alpha = 0.005$) under different steady flows with the water table at the toe elevation ($z_0 = 0$). The normalized flow rate q/k_s represents the intensity of the steady flow. Fig. 2(a) displays the profile of suction. It can be seen that the value of suction stress is zero when $q/k_s = -1$, which indicates that the backfill is saturated under this flow intensity. With increase of q/k_s from -1 to 1 (from infiltration to evaporation), the absolute values of suction increase obviously. Fig. 2 (b) is the profile of effective unit weight with different q/k_s. And it can be seen that the soil is saturated when $q/k_s = -1$ because the value of effective unit weight γ' is equal to saturated unit weight $\gamma_{sat} = 20\ \mathrm{kN/m^3}$. Compared with the suction, the values of effective unit weight gradually decrease as q/k_s varies from infiltration to evaporation and approximates the dry unit weight of the backfill. Above analyses show the pronounced effects of flow conditions on the hydraulic and mechanical response of unsaturated clay backfills, which highlights the importance of considering the flow condition in evaluation of the passive earth pressure of the retaining structures.

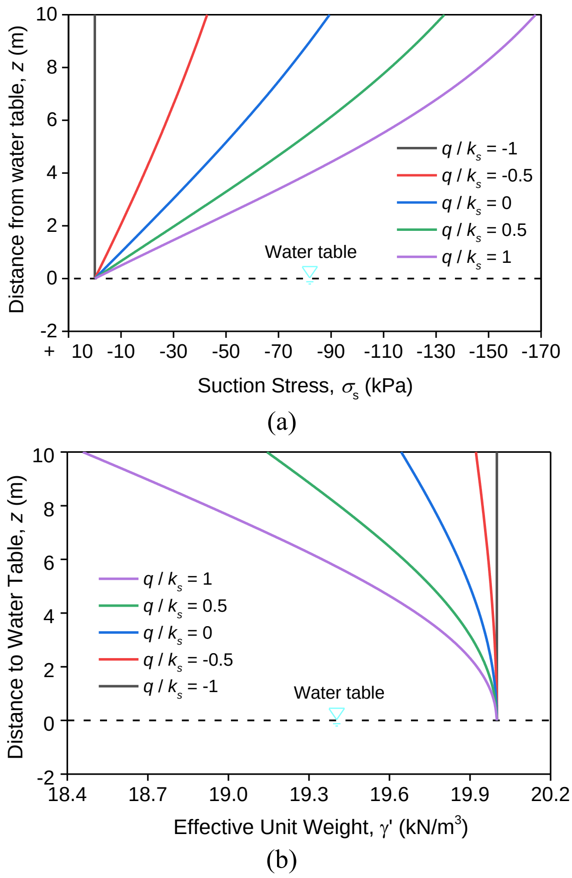

Fig. 2 Spatial distributions of (a) suction and (b) effective unit weight of clay backfill ($n = 2$, $\alpha = 0.005$) under different steady flows

3. General solutions formulation of passive resistance of retaining structure

The log-spiral slip surface is a wide-recognized failure mechanism for slope stability analysis. Ebrahimi (2011) conducted a limit analysis (LE) using the log-spiral slip failure model to investigate the active lateral seismic earth pressure coefficient. Following Ebrahimi's study, Vahedifard *et al.* (2015) further incorporated the effect of

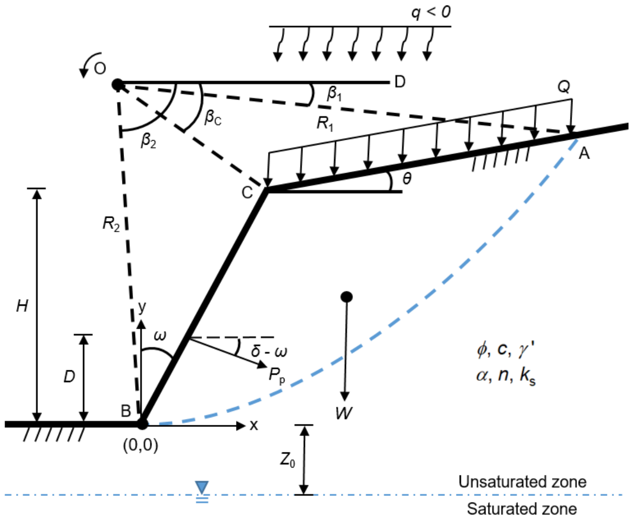

Fig. 3 Notation and convention for analysis of passive lateral earth pressure

suction into the log-spiral failure model and proposed a closed-form solution for the active pressure acting on retaining structures. Different from the failure model for active earth pressure, the log-spiral failure model for passive earth pressure is opposite to that for active state. Fig. 3 shows the notations and the failure mechanism for passive earth pressure of the retaining structures. As seen in Fig. 3, log-spiral failure surface rotates from the slope toe to the slope back surface, which is opposite to that of active case. The radius of the log-spiral failure surface can be mathematically expressed as

$$R = A\exp(-\psi\beta) \tag{9}$$

where R is the radius of log-spiral; β is the rotational angle of log-spiral, which varies from β_1 to β_2. ψ is a constant equal to $\tan\phi$, and ϕ is the internal friction angle of the backfill. A is a parameter of the log-spiral surface, which is given as

$$A = \frac{H(1-\tan\omega\tan\theta)}{[\exp(-\psi\beta_2)(\sin\beta_2+\tan\theta\cos\beta_2)-\exp(-\psi\beta_1)(\sin\beta_1+\tan\theta\cos\beta_1)]} \tag{10}$$

where H is the height of retaining structure; θ is the back slope angle and ω indicates the wall batter, which is the angle from the surface of the slope BC to the axis y; R_1 and R_2 represent the length of OA and OB, respectively, which can be determined by Eq. (9). Note that the radius of log-spiral for the passive situation increases from the toe to the crest of slope, which is opposite to the failure mechanism developed by Vahedifard *et al.* (2015) in the analysis of the active earth pressure.

Following the classical earth pressure theory, the resultant force of passive earth pressure, P_p, can be expressed as

$$P_\mathrm{p} = \frac{1}{2}K_\mathrm{p}\bar{\gamma}'H^2 \tag{11}$$

where K_p is the passive earth pressure coefficient; $\bar{\gamma}'$ indicates the average effective unit weight of soil along the height of the retaining structure, which is calculated as

$$\bar{\gamma}' = \frac{1}{H}\int_0^H \gamma'\mathrm{d}z \tag{12}$$

As shown in Fig. 3, the resultant force P_p acts at a certain height D above the toe elevation within the range between $H/3$ and $H/2$ (Craig 2004). The angle between the horizontal plane and the direction of P_p is $\delta-\omega$, where δ is the interface friction angle at the surface of retaining structure.

Based on the kinematic limit analysis method, the external work of the passive earth pressure should be equal to the work of internal energy dissipation that is provided by the suction, the unit weight, the cohesion and the surcharge at the back of the slope, which gives

$$W_{P_\mathrm{p}} = W_{\sigma^\mathrm{s}} + W_\mathrm{W} + W_\mathrm{c} + W_\mathrm{Q} \tag{13}$$

where W_{P_p} is the external work of the passive earth pressure; W_{σ^s} is the internal energy dissipation provided by suction σ^s; W_W is internal energy dissipation provided by the total weight of the block ABC; W_c is internal energy dissipation provided by the cohesive strength c along the failure surface AB; W_Q is internal energy dissipation provided by the uniform surcharge Q.

According to the geometrical relationships shown in Fig. 3, the expressions of the external work and internal energy dissipations can be derived as.

1) The external work of W_{P_p}

$$W_{P_\mathrm{p}} = P_\mathrm{p}\{\cos(\delta-\omega)\,[R_2\sin(\beta_2)-D] - \sin(\delta-\omega)[R_2\cos(\beta_2)-D\tan\omega]\} \tag{14}$$

2) The internal energy dissipation of W_{σ^s}

$$W_{\sigma^\mathrm{s}} = \int_{\beta_1}^{\beta_2}\sigma^\mathrm{s}A\,e^{-2\psi\beta}\cos\beta(-\psi\cos\beta+\sin\beta)\,\mathrm{d}\beta - \int_{\beta_1}^{\beta_2}\sigma^\mathrm{s}A\,e^{-2\psi\beta}\sin\beta(\cos\beta + \psi\sin\beta)\,\mathrm{d}\beta \tag{15}$$

3) The internal energy dissipation of W_W

$$W_\mathrm{W} = \int_{\beta_1}^{\beta_\mathrm{C}}\int_{d_1}^{R}\gamma' r^2\sin\beta\,\mathrm{d}r\mathrm{d}\beta + \int_{\beta_\mathrm{C}}^{\beta_2}\int_{d_2}^{R}\gamma' r^2\sin\beta\,\mathrm{d}r\mathrm{d}\beta \tag{16}$$

where β_C is the angle of COD; d_1 and d_2 are distance from point O to the surface AC and BC respectively. r is the distance from point O to certain point in block ABC. The explicit expressions of β_C, d_1 and d_2 can be derived from the geometrical relationships in Fig. 3 as

$$\beta_\mathrm{C} = \tan^{-1}\frac{R_2\sin\beta_2 - H}{H\tan\omega + R_2\cos\beta_2} \tag{17}$$

$$d_1 = \frac{R_1\sin(\beta_1+\theta)}{\sin(\beta+\theta)} \tag{18}$$

$$d_2 = \frac{R_2\sin\left(\frac{\pi}{2}-\beta_2+\omega\right)}{\sin\left(\frac{\pi}{2}+\beta-\omega\right)} \tag{19}$$

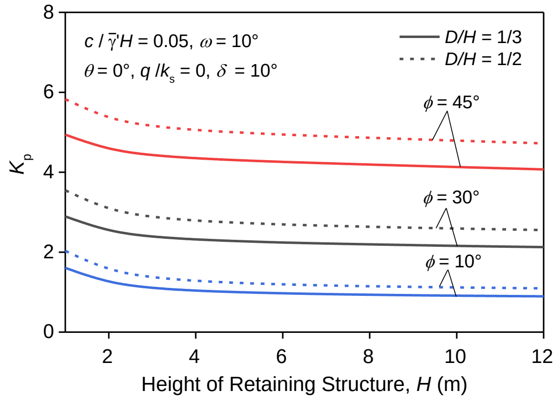

Fig. 4 Coefficient of passive earth pressure K_{p} versus height of retaining structure for different acting point of passive force

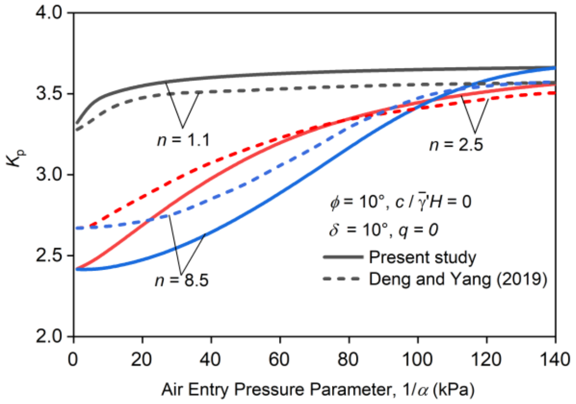

Fig. 5 Comparisons of coefficient of passive earth pressure K_{p} with Deng and Yang (2019)

4) The internal energy dissipation of W_{c}

$$W_{\mathrm{c}} = c\int_{\beta_1}^{\beta_2} A\, e^{-2\psi\beta} \sin\beta(-\psi\cos\beta + \sin\beta)\,\mathrm{d}\beta - c\int_{\beta_1}^{\beta_2} A\, e^{-2\psi\beta} \cos\beta(\cos\beta + \psi\sin\beta)\,\mathrm{d}\beta \tag{20}$$

5) The internal energy dissipation of W_Q

$$W_{\mathrm{Q}} = \frac{1}{2}Q(R_1\cos\beta_1 - R_2\cos\beta_2 - H\tan\omega)(R_1\cos\beta_1 + R_2\cos\beta_2 + H\tan\omega) \tag{21}$$

Substituting Eq. (11) into Eq. (13) and further arranging the equation, the expression of the passive earth pressure coefficient K_{p} can be expressed as the function of the variables β_1 and β_2 as follows

$$K_{\mathrm{p}} = f(\beta_1, \beta_2) = \frac{2(W_{\sigma^s} + W_{\mathrm{W}} + W_{\mathrm{C}} + W_{\mathrm{Q}})}{\bar{\gamma}' H^2\{\cos(\delta-\omega)[R_2\sin(\beta_2) - D] - \sin(\delta-\omega)[R_2\cos(\beta_2) - D\tan\omega]\}} \tag{22}$$

Since the passive earth pressure coefficient K_{p} are functions of two independent variables β_1 and β_2, a minimization procedure should be applied to determine the value of K_{p}. The minimum value of K_{p} from all the possible log-spiral slip surfaces should be the real passive earth pressure coefficient. In the searching procedure, the two independent variables β_1 and β_2 change sequentially with a small increment 0.001 in a single computational loop until β_1 varies from 0 to $\pi/2 + \omega$ and β_2 varies from β_1 to $\pi/2 + \omega$.

Generally, the acting point of the passive thrust lies within the range between $H/3$ and $H/2$, and $D = H/3$ is adopted in this study for conservative standpoint. Fig. 4 illustrates the passive earth pressure coefficient K_{p} versus the height of retaining structure for different acting point under no flow condition with $\omega = 10°$, $\theta = 0°$, and $\delta = 10°$. The soil layer of slope is clay ($n = 2, \alpha = 0.05\mathrm{kPa}^{-1}$) with the normalized cohesion value $c/\bar{\gamma}'H = 0.05$. The values of K_{p} are compared for $D = H/3$ and $D = H/2$ with different internal friction angles. As seen in Fig. 4, the value of K_{p} decreases with the increase of H, but the value for $H/3$ is obviously less than that for $H/2$. This figure proves that it's reasonable to adopt $D = H/3$ because it yields more conservative value of K_{p}, which ensures a safe design of the retaining structure.

4. Verification

To validate the accuracy and reliability of present method, Fig. 5 compares the K_{p} values calculated from present methods with the data extracted from Deng and Yang (2019). $\phi = 10°$, $c/\bar{\gamma}'H = 0$, $\delta = 10°$ and three different values of $n = 1.1, 2.5, 8.5$ are used to draw the figures. It should be noted that Deng and Yang (2019) proposed an analytical method for passive earth pressure based on the planar slip mechanism, while the present study employs log-spiral slip surface. Hence the comparison with Deng and Yang (2019) could show the accuracy and advantage of present method in calculation of the passive earth pressure.

As seen in Fig. 5, the K_{p} curves from present method share similar pattern with those Deng and Yang (2019) for all the cases involved, which show the reliability of present method. However, the coefficient of passive earth pressure K_{p} is larger than that of Deng and Yang (2019) for $n = 1.1$, while the coefficient of passive earth pressure K_{p} is smaller than that of Deng and Yang (2019) for $n = 1.1$ and 8.5. This indicates that the planar slip mechanism would underestimate the coefficient of passive earth pressure K_{p} for backfill with smaller n value, while overestimate the coefficient of passive earth pressure K_{p} for larger n value. Since the log-spiral slip surface is more reasonable than the planar slip mechanism (Michalowski and Drescher 2009), the comparison demonstrates that the present method would predict more accurate results in assessing the coefficient of passive earth pressure K_{p}.

5. Results and discussions

5.1 Effect of internal friction angle

Fig. 6 shows the passive earth pressure coefficient K_{p} versus the internal friction angle ϕ under different flow conditions for $H = 12\mathrm{m}$, $\omega = 10°$, $\theta = 0°$, and $\delta = 10°$.

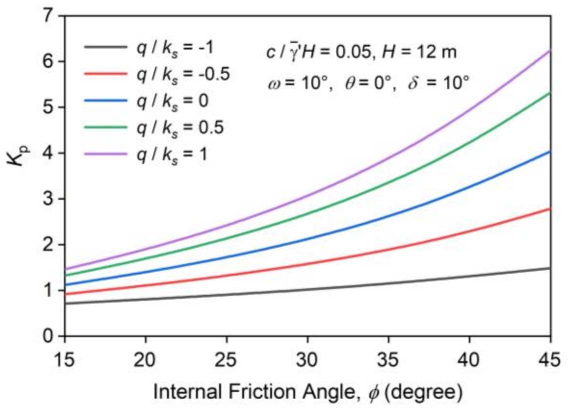

(a)

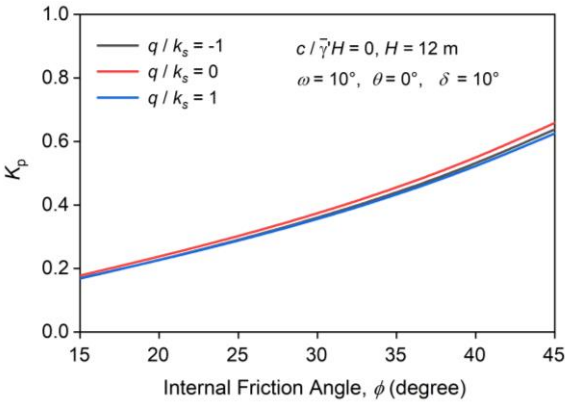

(b)

Fig. 6 Coefficient of passive earth pressure K_{p} versus internal friction angle ϕ under different flow conditions: (a) Clay backfill ($n = 2, \alpha = 0.05\mathrm{kPa}^{-1}, k_{\mathrm{s}} = 5 \times 10^{-8}\mathrm{m/s}$) and (b) Sand backfill ($n = 5, \alpha = 0.1\mathrm{kPa}^{-1}, k_{\mathrm{s}} = 3 \times 10^{-5}\mathrm{m/s}$)

The normalized cohesion $c/\bar{\gamma}'H$ are 0.05 and 0 for clay ($n = 2, \alpha = 0.05\ \mathrm{kPa}^{-1}, k_{\mathrm{s}} = 5 \times 10^{-8}\mathrm{m/s}$) and sand ($n = 5, \alpha = 0.1\ \mathrm{kPa}^{-1}, k_{\mathrm{s}} = 3 \times 10^{-5}\mathrm{m/s}$), respectively. It should be noted that the hydraulic conductivity k_{s} varies with the soil type and void ratio of the soil, and thus different k_{s} values are used for clay and sand in the analysis. Since the present study primarily focuses on the passive earth pressure under different steady-infiltration/evaporation conditions, the hydraulic conductivity k_{s} is assumed to be a constant for the same kind of soils for simple. It can be observed from Fig. 6(a) and 5(b) that the values of K_{p} for clay and sand increase with the internal friction angle ϕ for different flow conditions. The variations conform to the classical theories of earth pressure like Rankine’s or Coulomb’s theory (Craig 2004). Moreover, the value of K_{p} for clay in Fig. 6(a) increases significantly as the normalized flow rate q/k_{s} changes from -1 to 1. This indicates that the change of the flow condition from infiltration to evaporation has a significant effect on the passive resistance of the retaining structures. For example, for the case $\phi = 45°$, the value of K_{p} varies from 1.489 for $q/k_{\mathrm{s}} = -1$ to 6.255 for $q/k_{\mathrm{s}} = 1$, which indicates evaporation contributes to the significant increase of passive earth pressure behind retaining structure.

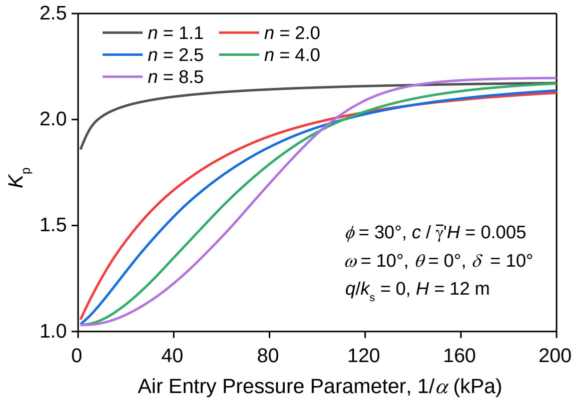

(a)

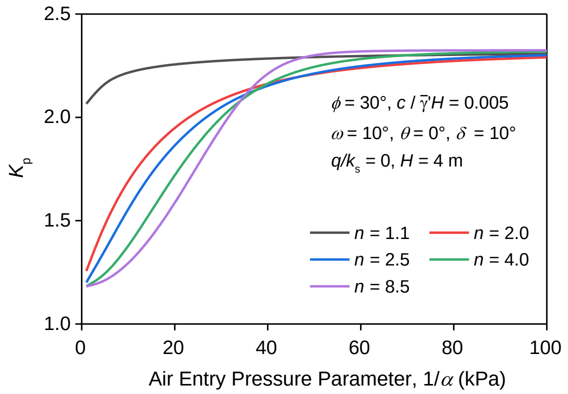

(b)

Fig. 7 Coefficient of passive earth pressure K_{p} versus air entry pressure $1/\alpha$ for different values of n (a) $H = 4$ m and (b) $H = 12$ m

However, as seen in Fig. 6(b), the curves of K_{p} for different q/k_{s} almost overlap each other, which implies that the flow condition has an almost negligible effect on the passive resistance of the retaining structures. Compared with the active earth pressure K_{a} investigated by Vahedifard *et al.* (2015), the variations of K_{p} for different flow conditions are opposite to the variations of K_{a}, as the failure mechanisms of these two kinds of earth pressures are completely opposite as discussed previously.

5.2 Effect of air entry pressure parameter and pore size distribution

Fig. 7 shows the passive earth pressure coefficient K_{p} versus the air entry pressure parameter $1/\alpha$ for $n = 1.1$, 2.0, 2.5, 4.0 and 8.5 under no flow condition. The heights of retaining structure H are 4 m and 12 m, respectively, for Fig. 7(a) and Fig. 7(b). Other parameters are shown in figures, i.e., $\phi = 30°$, $c/\bar{\gamma}'H = 0.05$, $\omega = 10°$, $\theta = 0°$, and $\delta = 10°$.

As seen in Figs. 7(a) and 7(b), the value of K_{p} increases with the air entry pressure parameter $1/\alpha$ and gradually approaches constant values. This is because that the air entry pressure parameter $1/\alpha$ is positive correlation with the suction σ^{s}, as shown by Eq. (4), and hence the larger value of the air entry pressure parameter $1/\alpha$ results in larger K_{p}. Vahedifard *et al.* (2015)

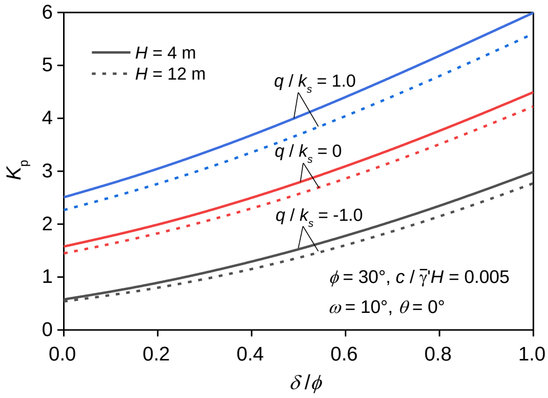

Fig. 8 Coefficient of passive earth pressure K_{p} versus ratio of interface friction angle δ to internal friction angle ϕ for different H

proposed that the lateral earth pressure does not increase infinitely with increase of $1/\alpha$ because the contribution from matric suction is limited, which also well explained that the values of K_{p} will approximates a constant finally. As stated previously, the parameter n in fact reflects the pore size distribution of the soil and the smaller value of n corresponds to larger value of σ^{s} (Lu *et al.* 2010). Hence, it can be seen that the value of K_{p} decreases with the increase of the value of n when the value of $1/\alpha$ is relatively small. For a higher retaining structure in Fig. 7(b) ($H = 12$ m), the variations of K_{p} with $1/\alpha$ and n are similar to those in Fig. 7(a), but the values of K_{p} are smaller, which indicates that the passive resistance of the retaining structure decreases with the height of the retaining structure.

5.3 Effect of interface friction angle

Fig. 8 shows the passive earth pressure coefficient K_{p} versus the ratio of interface friction angle δ to the internal friction angle of the backfill ϕ for different retaining structure heights H and flow conditions q/k_{s}. The geometrical parameters of the slope investigated are given as $\omega = 10°$ and $\theta = 0°$. The soil layer of slope is clay ($n = 2, \alpha = 0.05\mathrm{kPa}^{-1}$) with $\phi = 30°$ and $c/\bar{\gamma}'H = 0.005$.

As seen in Fig. 8, the K_{p} value increases substantially with the interface friction angle δ for all the cases considered, which indicates the interface friction angle δ has a pronounced effect on the passive earth pressures. Comparing the curves with different q/k_{s}, it can be observed that the K_{p} value increases more significantly with interface friction angle δ for the case $q/k_{\mathrm{s}} = 1$ and $H = 4$ m. This demonstrates that the effect of δ on K_{p} is impacted by the flow conditions and the height of the retaining structure. The above observations show that the coefficient of passive earth pressure K_{p} depends on many factors, such as the interface friction angle, the height of the retaining structure and the flow conditions. Therefore, a reasonable evaluation of the passive earth pressure should comprehensively consider these important factors.

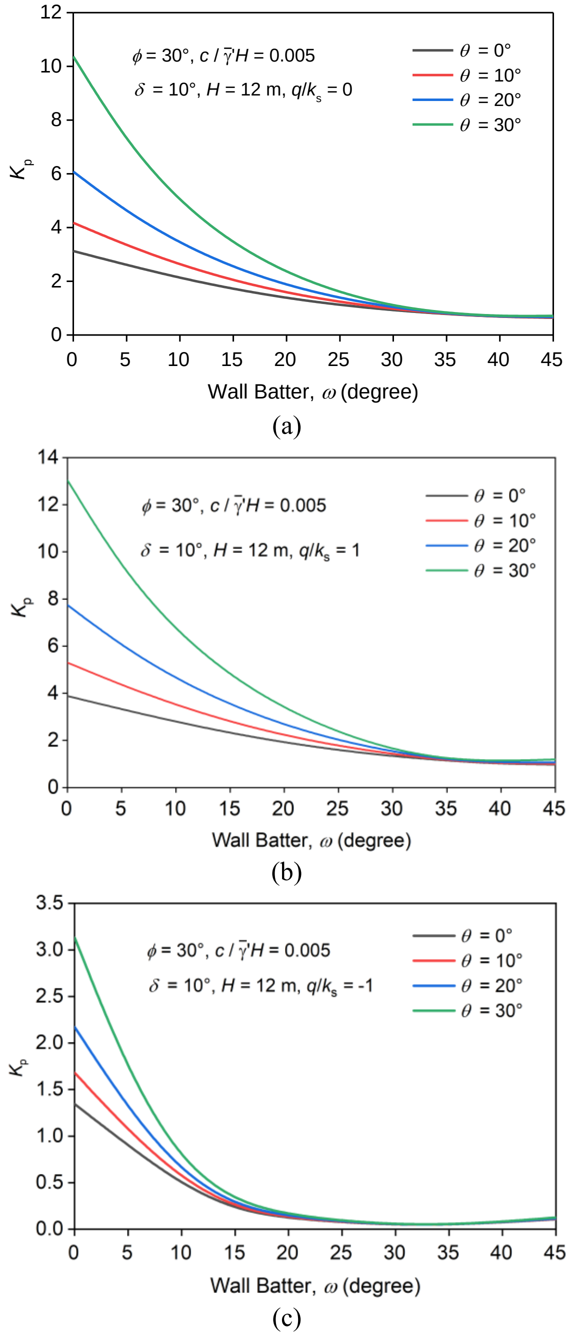

Fig. 9 Coefficient of passive earth pressure K_{p} versus wall batter ω for different back slope angles θ (a) $q/k_{\mathrm{s}} = 0$, (b) $q/k_{\mathrm{s}} = 1$ and (c) $q/k_{\mathrm{s}} = -1$

5.4 Effect of wall batter and back slope angle

Fig. 9 shows the passive earth pressure coefficient K_{p} versus the wall batter ω for different back slope angles θ for clay ($n = 2$, $\alpha = 0.05$ kPa^{-1}, $\phi = 30°$, $c/\bar{\gamma}'H = 0.005$) under three different flow conditions. The height of retaining wall and interface friction angle are 12 m and 10°, respectively. As seen in the figure, K_{p} gradually decreases with the increase of the wall batter ω and reaches a constant at certain ω, which suggests that the vertical retaining structure yields the minimum passive

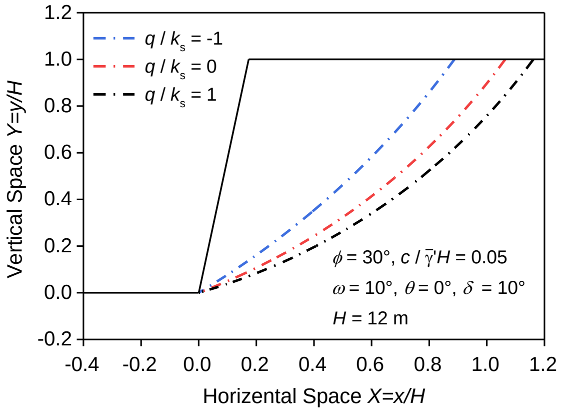

Fig. 10 Slip critical surface on three flow conditions

earth pressure. Different with ω, the slopes with larger θ show larger values of K_p because the weight of soil can provide greater resistance with the increase of back slope angle. However, the effects of θ become unapparent for larger wall batter ω since the curves with different θ almost approach the same value of K_p finally. For different flow conditions, the evaporation yields larger values of K_p than the infiltration, which is consistent with previous analysis of Vahedifard *et al.* (2015).

5.5 Effect of flow conditions on critical slip surface

According to the above results, it is clear that the flow conditions impose significant influence on the value of passive earth pressure. To further investigate the effects of flow condition on the failure mechanism, Fig. 10 plots the potential failure surface in the unsaturated backfill under different flow conditions q/k_s for clay backfill ($n = 2$, $\alpha = 0.05\text{kPa}^{-1}$, $\phi = 30°$, $c/\bar{\gamma}'H = 0.05$) with $H = 10\text{m}$. The other parameters are shown in the figures, i.e., $\omega = 10°$, $\theta = 0°$, and $\delta = 10°$. It can be seen that the slip surface enlargers with q/k_s increases from -1 to 1, which corresponding to the flow condition changes from infiltration to evaporation. Since the evaporation results in the increase of suction, the critical slip surface develops deeper in backfill and larger critical passive earth pressure is required to compensate the internal energy dissipation by the increased suction.

6. Conclusions

This paper theoretically investigates the passive resistance of retaining structures considering the unsaturation of the backfill under different flow conditions. The changes of both the suction and unit weight of the backfill due to infiltration and evaporation are considered in the present analysis. The coefficient of the passive earth pressure is determined from the log-spiral failure mechanism based on the kinematic limit analysis. According to the results, the following conclusions can be drawn:

1) The effects of flow conditions on passive earth pressure are obvious for clay backfills, which results from the variation of suction with flow conditions. Specifically, the evaporation/infiltration would greatly increase/reduce the suction, and hence improve/reduce the passive earth pressures. However, the changes of flow conditions impose almost no influence on the suction of sand backfill, and hence the passive earth pressures vary insignificant under different flow conditions for the retaining structures with sandy backfills.

2) For clayey backfills, the potential critical failure surface gradually extends deeper as the flow condition changes from infiltration to evaporation. Correspondingly, the passive resistance of the retaining structure increases substantially when the flow condition changes from infiltration to evaporation, as more external work is required to compensate the dissipation of the internal energy by the increased suction.

3) The geometrical parameters of slope and the properties of the backfill have significant effects on the coefficient of passive earth pressure. The coefficient of passive earth pressure generally increases with the internal friction angle, the back slope angle, the air entry pressure parameter, while decreases with the wall better and the height of the retaining structure.

Acknowledgments

The research described in this paper was financially supported by the National Natural Science Foundation of China (Grant No. 41772290).

References

Craig, R.F. (2004), *Craig's Soil Mechanics*, 7th Edition, Spon Press, London, England, U.K.

Damiano, E., Olivares, L. and Picarelli, L. (2012), "Steep-slope monitoring in unsaturated pyroclastic soils", *Eng. Geol.*, **137-138**(6), 1-12. https://doi.org/10.1016/j.enggeo.2012.03.002.

Deng, B. and Yang, M. (2019), "Analysis of passive Earth pressure for unsaturated retaining structures", *Int. J. Geomech.*, **19**(12), 06019016.
https://doi.org/10.1061/(ASCE)GM.1943-5622.0001518.

Ebrahimi, S. (2011), "Extension of Mononobe-Okabe approach to unstable slopes", M.Sc. Thesis, University of Delaware, Newark, Delaware, U.S.A.

Fathipour, H., Siahmazgi, A.S., Payan, M. and Chenari, R.J. (2020), "Evaluation of the lateral earth pressure in unsaturated soils with finite element limit analysis using second-order cone programming", *Comput. Geotech.*, **125**, 103587.
https://doi.org/10.1016/j.compgeo.2020.103587.

Gao, Y.F., Wu, D., Zhang, F., Lei, G.H., Qin, H. and Qiu, Y. (2016), "Limit analysis of 3D rock slope stability with non-linear failure criterion", *Geomech. Eng.*, **10**(1), 59-76.
https://doi.org/10.12989/gae.2016.10.1.059.

Gao, Y.F., Zhang, F., Lei, G.H. and Li, D.Y. (2013), "An extended limit analysis of three-dimensional slope stability", *Géotechnique*, **63**(6), 518-524.
https://doi.org/ 10.1680/geot.12.T.004.

Gardner, W.R. (1958), "Some steady state solutions of the unsaturated moisture flow equation with application to evaporation from a water table", *Soil Sci.*, **85**(4), 228-232.

https://doi.org/10.1097/00010694-195804000-00006.
Godt, J.W., Baum, R. and Lu, N. (2009), “Landsliding in partially saturated materials”, *Geophys. Res. Lett.*, **36**(2), L02403. https://doi.org/10.1029/2008GL035996.
Keskin, M.S. and Laman, M. (2014), “Experimental study of bearing capacity of strip footing on sand slope reinforced with tire chips”, *Geomech. Eng.*, **6**(3), 249-262. https://doi.org/10.12989/gae.2014.6.3.249.
Kim, S.K. and Borden, R.H. (2013), “Numerical simulation of MSE wall behavior induced by surface-water infiltration”, *J. Geotech. Geoenviron. Eng.*, **139**(12), 2110-2124. https://doi.org/10.1061/(ASCE)GT.1943-5606.0000927.
Koerner, R.M. and Koerner, G.R. (2013), “A data base, statistics and recommendations regarding 171 failed geosynthetic reinforced mechanically stabilized earth (MSE) walls”, *Geotext. Geomembranes*, **40**, 20-27. https://doi.org/10.1016/j.geotexmem.2013.06.001.
Krabbenhoft, K. (2017), “Static and seismic earth pressure coefficients for vertical walls with horizontal backfill”, *Soil Dyn. Earthq. Eng.*, **104**, 403-407. https://doi.org/10.1016/j.soildyn.2017.11.011.
Lim, K., Li, A.J. and Lyamin, A.V. (2015), “Three-dimensional slope stability assessment of two-layered undrained clay”, *Comput. Geotech.*, **70**, 1-17. https://doi.org/10.1016/j.compgeo.2015.07.011.
Lu, N. and Likos, W.J. (2004), *Unsaturated soil mechanics*, Wiley, New York, U.S.A.
Lu, N. and Likos, W.J. (2006), “Suction stress characteristic curve for unsaturated soil”, *J. Geotech. Geoenviron. Eng.*, **132**(2), 131-142. https://doi.org/10.1061/(ASCE)1090-0241(2006)132:2(131).
Lu, N., Godt, J.W. and Wu, D.T. (2010), “A closed-form equation for effective stress in unsaturated soil”, *Water Resour. Res.*, **46**(5), 1-142. https://doi.org/10.1029/2009WR008646.
Lu, N., Kaya, M., Collins, B.D. and Godt, J.W. (2013), “Hysteresis of unsaturated hydromechanical properties of a silty soil”, *J. Geotech. Geoenviron. Eng.*, **139**(3), 507-510. https://doi.org/10.1061/(ASCE)GT.1943-5606.0000786.
Michalowski, R.L. and Drescher, A. (2009), “Three-dimensional stability of slopes and excavations” *Géotechnique*, **59**(10), 839-850. https://doi.org/10.1680/geot.8.P.136.
Mualem, Y. (1976), “A new model for predicting hydraulic conductivity of unsaturated porous media”, *Water Resour. Res.*, **12**(3), 513-522. https://doi.org/10.1029/wr012i003p00513.
Prakash, K., Sridharan, A., Thejas, H.K. and Swaroop, H.M. (2012), “A simplified approach of determining the specific gravity of soil solids”, *Geotech. Geol. Eng.*, **30**(4), 1063-1067. https://doi.org/10.1007/s10706-012-9521-6.
Rahardjo, H., Rezaur, R.B., Leong, E.C., Alonso, E.E., Lloret, A. and Gens, A. (2008), “Monitoring and modeling of slope response to climatic changes”, *Proceedings of the 10th International Symposium on Landslides and Engineered Slopes*, Xi’an, China, June-July.
Sahoo, J.P. and Ganesh, R. (2017), “Active earth pressure on retaining walls with unsaturated soil backfill”, *Proceedings of the International Congress and Exhibition “Sustainable Civil Infrastructures: Innovative Infrastructure Geotechnology*, Sharm Elsheikh, Egypt, July.
Vahedifard, F., Leshchinsky, B.A., Mortezai, K. and Lu, N. (2015), “Active earth pressures for unsaturated retaining structures”, *J. Geotech. Geoenviron. Eng.*, **141**(11), 04015048. https://doi.org/10.1061/(ASCE)GT.1943-5606.0001356.
Vahedifard, F., Leshchinsky, B.A., Sehat, S. and Leshchinsky, D. (2014), “Impact of cohesion on seismic design of geosynthetic-reinforced earth structures”, *J. Geotech. Geoenviron. Eng.*, **140**(6), 04014016. https://doi.org/10.1061/(ASCE)gt.1943-5606.0001099.
Vahedifard, F., Leshchinsky, D., Mortezaei, K. and Lu, N. (2016), “Effective stress-based limit-equilibrium analysis for homogeneous unsaturated slopes”, *Int. J. Geomech.*, **16**(6), 04016003. https://doi.org/10.1061/(ASCE)GM.1943-5622.0000554.
Valentine, R.J. (2013), “An assessment of the factors that contribute to the poor performance of geosynthetic-reinforced earth retaining walls”, *Proceedings of the International Symposium on Design and Practice of Geosynthetic-Reinforced Soil Structures,* Bologna, Italy, October.
Van Genuchten, M.Th. (1980), “A closed-form equation for predicting the hydraulic conductivity of unsaturated soils”, *Soil Sci. Soc. Am. J.*, **44**(5), 892-898. https://doi.org/10.2136/sssaj1980.03615995004400050002x.
Veiskarami, M., Jamshidi Chenari, R. and Jameei, A.A. (2018), “A study on the static and seismic earth pressure problems in anisotropic granular media”, *Geotech. Geol. Eng.*, **37**(3), 1987-2005. https://doi.org/10.1007/s10706-018-0739-9.
Yamaguchi, K., Takeuchi, N. and Hamasaki, E. (2018), “Three-dimensional simplified slope stability analysis by hybrid-type penalty method”, *Geomech. Eng.*, **15**(4), 947-955. https://doi.org/10.12989/gae.2018.15.4.947.
Yang, X.L. and Liu Z.A. (2018), “Reliability analysis of three-dimensional rock slope”, *Geomech. Eng.*, **15**(6), 1183-1191. https://doi.org/10.12989/gae.2018.15.6.1183.
Yang, X.L. and Xu, J.S. (2017), “Three-dimensional stability of two-stage slope in inhomogeneous soils”, *Int. J. Geomech.*, **17**(7), 06016045. https://doi.org/10.1061/(ASCE)GM.1943-5622.0000867.
Yoo, C. and Jung, H. (2006), “Case history of geosynthetic reinforced segental retaining wall failure”, *J. Geotech. Geoenviron. Eng.*, **132**(12), 1538-1548. https://doi.org/10.1061/(ASCE)1090-0241(2006)132:12(1538).

CC